More than three-fold increase in compound soil and air dryness across Europe by the end of 21st century

Journal Article

Author(s):
Shekhar, Ankit; Buchmann, Nina; Humphrey, Vincent; Gharun, Mana

Publication date:
2024-06

Permanent link:
https://doi.org/10.3929/ethz-b-000668478

Originally published in:
Weather and Climate Extremes 44, https://doi.org/10.1016/j.wace.2024.100666

Funding acknowledgement:
ETH-27 19-1 - Forest Vulnerability to Extreme and Repeated Climatic Stress (FEVER) (ETHZ)
198094 - Unravel the changing contributions of abiotic vs. biotic drivers of ecosystem gas exchange under weather extremes (SNF)

Weather and Climate Extremes 44 (2024) 100666

Contents lists available at ScienceDirect

Weather and Climate Extremes

journal homepage: www.elsevier.com/locate/wace

More than three-fold increase in compound soil and air dryness across Europe by the end of 21st century

Ankit Shekhar [a,*], Nina Buchmann [a], Vincent Humphrey [b], Mana Gharun [c]

[a] Department of Environmental Systems Science, ETH Zürich, 8092 Zürich, Switzerland
[b] Federal Office of Meteorology and Climate MeteoSwiss, Zürich, Switzerland
[c] Faculty of Geosciences, University of Münster, 48149 Münster, Germany

ARTICLE INFO

Keywords:
Soil moisture
Vapor pressure deficit
EURO-CORDEX
ERA5-Land
E-OBS

ABSTRACT

Increases in air temperature lead to increased dryness of the air and potentially develops increased dryness in the soil. Extreme dryness (in the soil and/or in the atmosphere) affects the capacity of ecosystems for functioning and for modulating the climate. Here, we used long-term high temporal resolution (daily) soil moisture (SM) and vapor pressure deficit (VPD) data of high spatial resolution (~0.1° × 0.1°) to show that compared to the reference period (1950–1990), the overall frequency of extreme soil dryness, extreme air dryness, and extreme compound dryness (i.e., co-occurrence of extreme soil dryness and air dryness) has increased by 1.2-fold [0.8,1.6] (median [10th,90th percentile], 1.6-fold [1,2.3], and 1.7-fold [0.9,2.5], respectively, over the last 31 years (1991–2021) across Europe. Our results also indicate that this increase in frequency of extreme compound dryness (between reference and 1991–2021 period) is largely due to increased SM-VPD coupling across Northern Europe, and due to decreasing SM and/or increasing VPD trend across Central and Mediterranean Europe. Furthermore, under the RCP8.5 (Representative Concentration Pathways 8.5) emission scenario, this increase in frequency of extreme compound dryness would be 3.3-fold [2.0,5.8], and 4.6-fold [2.3,11.9] by mid-21st century (2031–2065) and late-21st century (2066–2100), respectively. Additionally, we segregated the changes in frequency of extreme dryness across the most recent (year 2021) land cover types in Europe to show that croplands, broadleaved forest, and urban areas have experienced more than twice as much extreme dryness during 1990–2021 compared to the reference period of 1990–2021, which based on the future projection data will increase to more than three-fold by mid 21st century. Such future climate-change induced increase in extreme dryness could have negative implications for functioning of ecosystems and compromise their capacity to adapt to rapidly rising dryness levels.

1. Introduction

Our Earth has been experiencing an unprecedented rate of warming since the start of the 20th century. According to a report from "Copernicus Climate Indicators", global mean air temperature has increased by 1.2 °C since the pre-industrial period of 1850–1900, whereas surface air temperature over Europe has increased by 2.2 °C (https://climate.copernicus.eu/climate-indicators/temperature). In the absence of additional precipitation, warming over land leads to increased air dryness (measured by vapor pressure deficit, VPD) which can lead to increased evapotranspiration (ET) and a faster soil drying (Teuling, 2018; Yin et al., 2014; Zhang et al., 2023). In addition, low precipitation will lead to low soil moisture (SM) if ET draws down available soil water pools. If both conditions co-occur, i.e., high VPD and low SM, a compound dry conditions, or even extreme compound dryness develop, i.e., co-occurrence of extreme high VPD values (e.g., VPD > 90th percentile; extreme air dryness) and extreme low SM levels (e.g., SM < 10th percentile; extreme soil dryness) (Seneviratne et al., 2012; Shekhar et al., 2024; Zscheischler and Seneviratne, 2017).

Although over the past 40 years, most parts of Europe have experienced persistent precipitation patterns (Lal et al., 2023), increasing ET, due to increased VPD might have resulted in soil drying trends, however the causation is difficult to establish (Lal et al., 2023). The impact of global warming has had profound devastating effects on Europe's land ecosystems, especially in the 21st century when it was impacted by drought and heatwaves (monthly, seasonal, or longer timescales) in

* Corresponding author.
E-mail address: ankit.shekhar@usys.ethz.ch (A. Shekhar).

https://doi.org/10.1016/j.wace.2024.100666
Received 16 September 2023; Received in revised form 16 February 2024; Accepted 22 March 2024
Available online 28 March 2024

2003, 2010, 2015, 2018, 2019, and the most recent in 2022 (Bastos et al., 2021; Hermann et al., 2023; Ionita et al., 2017; Markonis et al., 2021; Scapucci et al., 2024; Shekhar et al., 2020; Tripathy and Mishra, 2023). Such droughts and heatwaves mostly occur during the main European carbon uptake period (April–September) when the terrestrial ecosystem acts as a sink (Peters et al., 2010). The extreme high soil dryness and/or air dryness, occurring at daily or weekly scales, are the two main characteristics of such drought and heatwave events (Miralles et al., 2014, 2019) which directly impact water use and carbon uptake by terrestrial ecosystems (Fu et al., 2022; He et al., 2022; Humphrey et al., 2021; Liu et al., 2020; Novick et al., 2016; Yuan et al., 2019), already at daily timescales (Gou et al., 2024, 2024, 2024; Shekhar et al., 2024; Stoy et al., 2009; Yuan et al., 2016; Zhou et al., 2021). Although, much is known about the projections of drought and heatwaves in Europe (Markonis et al., 2021; Samaniego et al., 2018; Teuling, 2018), we know little about how extreme low SM and/or extreme high VPD days have changed since past and are projected to change in future, given their direct impact on ecosystem. Furthermore, the trend in soil and air drying across Europe could directly increase the frequency and intensity of extreme dryness, whereas it could also indirectly increase the SM and VPD covariance (coupling) which will further increase the frequency of extreme compound dryness in the future (Zhou et al., 2019a,b). A recent study by Zhou et al. (2019a) showed that the increase in frequency of extreme compound dryness during warm season is largely due to monthly increase in SM-VPD coupling. Little is known about how trends in daily SM and VPD, and their coupling have changed the intensity and frequency of these extreme compound dryness over the past decades and how they are projected to change in the future.

In this study we aim (i) to quantify how intensity and frequency of occurrences of extreme soil dryness, extreme air dryness and extreme compound dryness i.e., co-occurring extreme soil dryness AND extreme air dryness (all three collectively as extreme dryness) have changed across Europe since the 1950s, and how they are projected to change in the future until 2100; (ii) to quantify the changes in SM and VPD coupling and its impact on extreme compound dryness across Europe from 1950 to 2100. We hypothesize that the increase in frequency and intensity of extreme compound dryness would be largely due to increased SM-VPD coupling across Europe. We also segregate the changes quantified in (i) and (ii) across different land cover types to highlight changes in intensity and frequency of extreme dryness of the present land cover of Europe.

2. Methods

2.1. Vapor pressure deficit and soil moisture data from 1950 to 2021

The study area is Europe (Longitude: 11°W - 33°E; Latitude: 35.8°N-72°N), comprising of three distinct regions (Markonis et al., 2021), namely Northern Europe (NEU), Central Europe (CEU) and Mediterranean Europe (MED; Fig. S1). We used the E-OBS v26.0e dataset (Cornes et al., 2018; Klein Tank et al., 2002) is a Europe-wide, observation-based, daily, gridded (0.1° × 0.1°) meteorological dataset covering 1950 to 2021 (72 years). We used daily average temperature (Tg; °C) and relative humidity (RH; %) data from E-OBS in this study. We calculated vapor pressure deficit (VPD, kPa) from mean temperature and relative humidity using Eq. (1) (Jones, 2014).

$$VPD = \left(1 - \frac{RH}{100}\right) \times 0.6107 \times 10^{\frac{7.5 \times Tg}{237.3+Tg}} \quad (1)$$

We obtained the surface (0–7 cm depth) soil moisture (SM) data from the most recent reanalysis data from ECMWF's (European Centre for Medium-range Weather Forecasts) new land component of the fifth generation of European Reanalysis (ERA5-Land) dataset (Muñoz-Sabater et al., 2021) spanning over seven decades (1950–2021). The ERA5-Land uses the Tiled ECMWF Scheme for Surface Exchanges over Land with a revised land surface hydrology (HTESSEL) (Hersbach et al., 2020). The SM data from ERA5-Land is available at an hourly resolution with spatial resolution of 0.1° × 0.1°. We aggregated SM data from hourly values to daily means for our analysis. Recent in-situ and satellite based validation studies have shown high accuracy of surface SM simulation of ERA5-Land (Albergel et al., 2012; Lal et al., 2022; Muñoz-Sabater et al., 2021). We obtained both the ERA5-Land and E-OBS datasets from the climate data store of Copernicus Climate Change Service (https://cds.climate.copernicus.eu). Additionally, we also obtained the land cover data for the year 2021 from MODIS product MCD12Q1 Version 6.1 (Friedl and Sulla-Menashe, 2015), which gives yearly land cover information at 500 m resolution as per International Geosphere Biosphere Program (IGBP) classification: ENF – Evergreen needleleaf forest, EBF – Evergreen broadleaf forest, DBF – Deciduous broadleaf forest, MF – Mixed forest, OSH – Open shrublands, WSA – Wooden savannas, SAV – Savannas, GRA – Grasslands, CRO – Croplands, URB – Urban and built-up areas, CNV – Cropland and natural vegetations mosaics. In this study we masked out any barren land or water bodies. We then aggregated the land cover data to 0.1° × 0.1° resolution, by assigning the majority land cover types in each 0.1° × 0.1° grid.

2.2. Future projection data until 2100

We used the climatic projections of the EURO-CORDEX project (domain: EUR-11; http://www.euro-cordex.net) from 1950 to 2100 to project extreme compound dryness into the future. EURO-CORDEX is the European branch of the international CORDEX initiative, which is a program sponsored by the World Climate Research Program (WRCP) to organize an internationally coordinated framework to produce improved regional climate change projections for all land regions worldwide (Kotlarski et al., 2014; Vautard et al., 2021). EURO-CORDEX project offers simulation of high spatiotemporal resolution (daily at 0.11° × 0.11° resolution) that allow us to improve our understanding on past, present, and future evolution of extreme events. We used daily means of surface air temperature (i.e., tas, K), surface relative humidity (i.e., hurs, %), and total soil moisture content (i.e., mrso, kg/m^2) from a total 12 regional climate models (RCMs) using the boundary conditions from the five global climate model driven under the RCP8.5 (Representative Concentration Pathways 8.5) emission scenario as shown in Table S1. The RCP8.5 based future projections is widely used in recent studies focusing on future evolution of extreme events (Cardell et al., 2020; Molina et al., 2020; Schwalm et al., 2020; Zhou et al., 2019b). We calculated the daily VPD for the future projection from surface air temperature and relative humidity using Eq. (1).

2.3. Statistical analyses

All statistical data analyses carried out in this study were performed in R statistical programming language (R Core Team, 2021) and involved the following steps.

1. Since dryness extremes are relevant for terrestrial carbon cycle, we focused all our analyses on the during April–September months (183 days) as most of the carbon sink activity occurs during this period across Europe (Peters et al., 2010). We assumed 1950–1990 as a reference period (total 41*183 = 7503 days) and 1991–2021 as the present period (total 5673 days). We divided the future period into two slices of 35 years each: 2031–2065 (mid 21st century; 6405 days) and 2066–2100 (late 21st century; 6405 days) to quantify and compare the frequency and intensity of each type of extremes (extreme soil dryness, extreme air dryness and extreme compound dryness). Initial data preprocessing (calculation and daily aggregation of VPD) was done using CDO (climatic data operators) software (Schulzweida, 2022) and the '*raster*' R-package (Hijmans et al., 2014)

2. We detected trends (from 1950 to 2021) of yearly mean SM and VPD (mean SM and VPD of each year), and yearly 10th percentile SM (SM_{10P}; one for each year) and 90th percentile VPD (VPD_{90P}; one for each year) across Europe (i.e. for each 0.1° × 0.1° grid). The yearly trend was calculated by a modified Mann-Kendall trend test using the '*rtrend*' R-package, which accounts for the serial correlation in the time series data (Kong and Song, 2022).
3. We used the "peak over threshold" approach to identify extreme soil dryness ($SM < SM_{10P}$; 10th percentile SM), extreme air dryness ($VPD > VPD_{90P}$; 90th percentile VPD) and extreme compound dryness days ($SM < SM_{10P}$ AND $VPD > VPD_{90P}$) across Europe during each of the reference, present and future periods (Zhou et al., 2019b; Zscheischler and Seneviratne, 2017). The intensity of extremes was defined by the extreme SM and VPD thresholds, i.e., SM_{10P} and VPD_{90P}, for reference, present and future periods. Decrease in SM_{10P} (across different periods) implied increased intensity of extreme soil dryness, whereas increase in VPD_{90P} implied increased intensity of extreme air dryness and vice-versa.
4. We used bivariate copula to model the dependence structure of SM and VPD and calculate the occurrence probability of extreme compound dryness. Bivariate copulas are widely used to model the dependence between two random variables (here SM and VPD) with different marginal distributions (Genest and Favre, 2007). Based on our definition in step 3, the joint occurrence probability of extreme compound dryness (P_{CD}) is given by Eq. (2) for any time period (*tp*; reference, present, and future) with SM and VPD thresholds from any period (*th*; reference, present, and future).

$$\begin{aligned} P_{CD}[tp,th] &= P(SM[tp] < SM_{10P}[th] \cap VPD[tp] > VPD_{90P}[th]) \\ &= P(SM[tp] < SM_{10P}[th]) - P(SM[tp] < SM_{10P}[th] \cap VPD[tp] \le VPD_{90P}[th]) \\ &= P(SM[tp] < SM_{10P}[th]) - C_{tp}(SM_{10P}[th], VPD_{90P}[th]) \end{aligned} \quad (2)$$

where, C_{tp} is the cumulative distribution function of the bivariate copula estimated on any period, tp. The detailed theory about bivariate copulas can be found in the literature (Genest and Favre, 2007; Wable and Jha, 2018). Copula modeling was done for each grid for each different periods – e.g., for reference period we used SM and VPD data for 7503 days for each grid point to detect its SM_{10P} and VPD_{90P} to finally calculate P_{CD}. We considered commonly used copula families (Gaussian copula, Student's t copula, and Archimedean copula) and used the best fit copula based on the Bayesian Information Criterion to calculate P_{CD}. The copula analysis was performed using the "*VineCopula*" R package (Nagler et al., 2022), with which we used the function '*BiCopSelect*' to select the best fit copula function and then used function '*BiCopCDF*' to calculate the P_{CD}. We also compared our P_{CD} obtained from the copula method with P_{CD} obtained from a simple counting method (fraction of days exceeding the SM and VPD thresholds). We found negligible differences between the two methods (maximum and mean absolute differences of 2.1% and 0.05%, respectively). Such negligible differences were expected as we are analyzing daily data with little data limitation (>5000 days for each grid during reference, present and future periods). In this study, we describe all our P_{CD} based on the copula method as estimated with Eq. (2).

5. We calculated the probability multiplication factor (PMF) across Europe for different periods (reference, present and future) to quantify the change in occurrence probability of extreme compound dryness due to covariance of SM and VPD (Zhou et al., 2019a). PMF of any period is the ratio of P_{CD} (joint probability calculated by bivariate copula with thresholds of the corresponding periods) and 0.01 (assuming SM and VPD are independent = 0.1 × 0.1 = 0.01). Therefore, a value of PMF = 1 implies that there was no change in occurrence probability due to covariance of SM and VPD. PMF for any period (*tp*) was calculated as shown by Eq. (3).

$$PMF\ [tp] = \frac{P_{CD}[tp,th]}{0.01};\ th = tp = reference, present\ \&\ future \quad (3)$$

where both *tp* and *th* are of the same period.

6. Finally, to quantify changes in the occurrence probability of extreme compound dryness (ΔP_{CD}) in present and future periods (*tp* = present & future) relative to the reference period (*th* = reference), we used the extreme thresholds (SM_{10P} and VPD_{90P}) of the reference period to calculate P_{CD} (as per Eq. (2)), i.e., *th* = reference period, during the present period (1991–2021; tp = present) and two future periods (*tp* = mid 21st century and late 21st century) for E-OBS and ERA5-Land data (present period) each RCM model (for present and future comparisons) as shown in Eq. (4).

$$\Delta P_{CD}[tp] = \frac{P_{CD}[tp, reference]}{P_{CD}[reference, reference]};\ tp = present\ \&\ future \quad (4)$$

The ΔP_{CD} for any period present and future period (*tp*) can be segregated into ΔP_{CD} due to changes in SM-VPD coupling (ΔP_{CD} coupling) and changes in SM and/or VPD trend (ΔP_{CD} trend) as shown in Eqs. (5) and (6).

$$\Delta P_{CD}coupling\ [tp] = \frac{PMF\ [tp]}{PMF\ [reference]};\ tp = present\ \&\ future \quad (5)$$

$$\Delta P_{CD}trend\ [tp] = \frac{P_{CD}[tp, reference]}{0.01 \times PMF\ [tp]};\ tp = present\ \&\ future \quad (6)$$

Final present and future occurrence probability from all 12 RCM models were averaged to calculate the average change in probability of extreme compound dryness in present and future periods. We further performed the analysis from Step 1 to Step 5 at a monthly scale with mean monthly VPD and SM to compare the PMF from two different temporal scale.

3. Results

3.1. A drying europe

The majority of Central Europe (CEU) and Mediterranean Europe (MED) showed a significant negative trend in the yearly mean soil moisture (SM) in the topsoil (0–7 cm; April to September), while Northern Europe (NEU) has showed substantial soil wetting as indicated by the positive trend in SM (Fig. 1a) from 1950 to 2021. Except for southwestern Finland, yearly mean VPD (April to September) showed a significantly increasing trend between 1950 and 2021, with parts of southern Spain showed the highest positive trend of more than 0.1 kPa/decade (Fig. 1c). Additionally, we also explored the trends of the yearly extreme thresholds of SM and VPD, i.e., yearly SM_{10P} (10th percentile SM of each year) and VPD_{90P} (90th percentile VPD of each year). The patterns of yearly SM_{10P} and VPD_{90P} trends (Fig. 1b and d) were spatially similar but more pronounced than those of the yearly mean SM and VPD trends, respectively (Fig. 1a and c). The trends of SM_{10P} and VPD_{90P} were about 35% and 80% higher than those of yearly mean SM and VPD between 1950 and 2021, respectively (indicated by slope of the linear regression in Fig. S2). This indicated that the rate of intensification of extreme soil and air drying was higher than that mean drying. Therefore, we observed development of compound dry conditions characterized by both decreasing trend of SM and increasing trend of VPD across most of the CEU and MED over last 72 years (1950–2021).

3.2. Increase in extreme soil dryness and extreme air dryness

Compared to the reference period (1950–1990), the SM_{10P} threshold (indication of intensity of extreme soil dryness) of the present period (1991–2021) in CEU and MED was typically 15%–25% lower (i.e.,

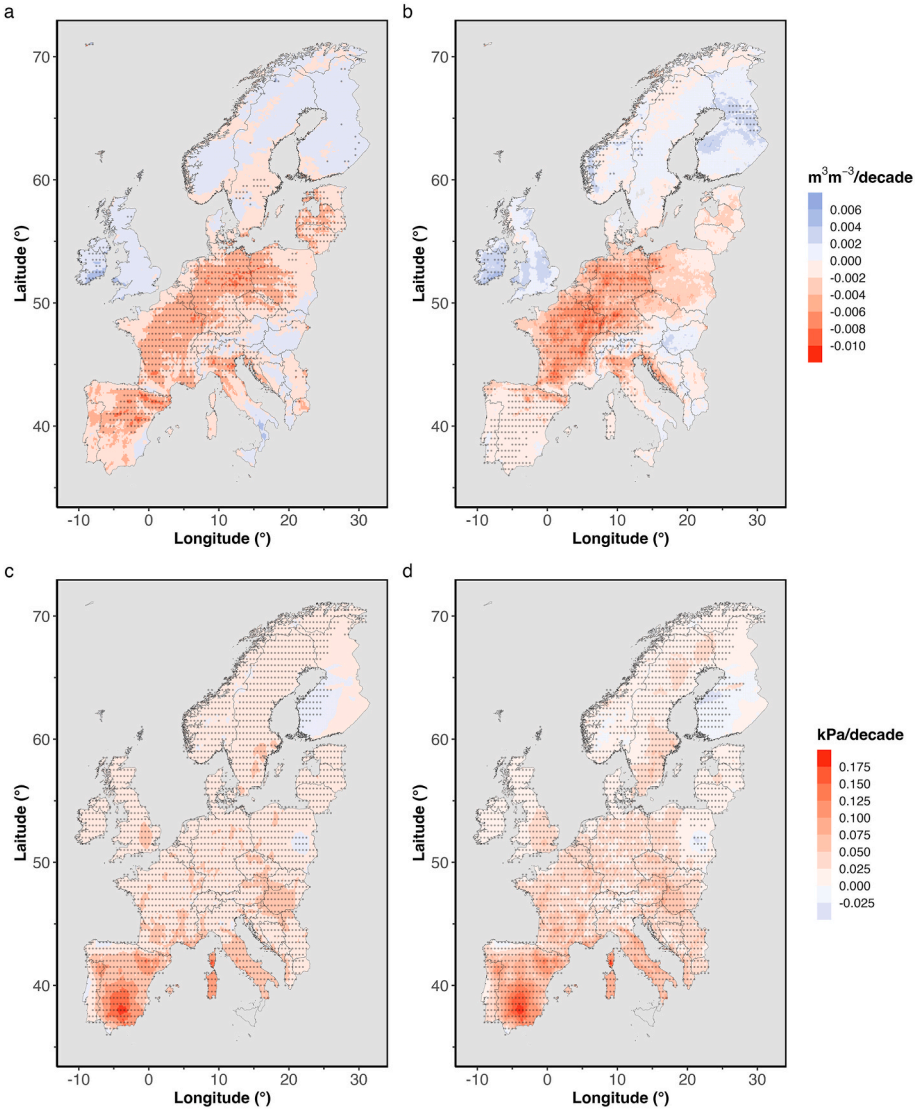

Fig. 1. Pronounced soil drying (a, b) and air drying (c, d) of Europe during the months April to September between 1950 and 2021 as demonstrated by negative trends of (a) yearly mean soil moisture, and (b) yearly 10th percentile soil moisture (SM_{10P}), and positive trends of (c) yearly mean VPD, and (d) yearly 90th percentile VPD (VPD_{90P}). The significant trend ($p < 0.05$) areas are marked by black dots based on a modified Mann-Kendall trend test (see Methods).

intensity of extreme soil dryness increased by 15–25 %). In contrast, the SM_{10P} in NEU was about 10% higher than that during the reference period (Fig. 2a), implying a 10% decrease in intensity of extreme soil dryness. The spatial pattern of change in frequency was similar to that of change in intensity of extreme soil dryness (Fig. 2a and b). The frequency of extreme soil dryness increased 1.2-fold [0.8,1.6] (median [10th, 90th percentile] (Fig. 2b) across Europe (compared to the reference), with most of CEU and MED showed more than a 1.5-fold increase in frequency of extreme soil dryness. Both increased in intensity and frequency of extreme soil dryness was prominent for urban areas, croplands, as well as broadleaved and mixed forests (Fig. 2c and d).

Except for Finland, the VPD_{90P} threshold (indication of intensity of extreme air dryness) of the present period was higher than that of the reference period across Europe (Fig. 3a). Overall, the increase in intensity of extreme air dryness across Europe was about 15%, with more than 50% increase in intensity for majority of MED (Fig. 3a). The spatial pattern of change in frequency was similar to that of change in intensity of extreme air dryness (Fig. 3a and b). The frequency of extreme air dryness largely increased across Europe (compared to the reference), with about 1.6-fold [1,2.3] increase (median [10th, 90th percentile] over Europe (Fig. 3b) and about one-quarter of Europe showing more than a two-fold increase in frequency of extreme air dryness during the present period in comparison to the reference period. Both increased in intensity and frequency of extreme air dryness was prominent (intensity >20% and frequency > two-fold) for urban areas, croplands, as well as broadleaved forests (Fig. 3c and d).

3.3. Daily SM-VPD coupling

Extreme compound dryness, i.e., the co-occurrence of extreme soil and air dryness not only relate to changes in either SM and VPD contributing to the compound extreme, but also to the relationship between SM and VPD. Daily topsoil SM and VPD values were significantly negatively correlated, indicating strong (negative) SM-VPD coupling across most of Europe during the reference and the present period (Fig. S3). Weak SM-VPD coupling [absolute r (SM,VPD) < 0.2] was observed at higher latitudes (>65°N), particularly at higher elevations (NEU), and in the Alpine region (CEU; Fig. S3a and b). Compared to the reference period (median r (SM,VPD) of −0.56), the present period showed a stronger SM-VPD coupling (median r (SM,VPD) of −0.63), with more than 80% of Europe showing stronger SM-VPD coupling, largely consistent across land cover types (Fig. 4). This increase in

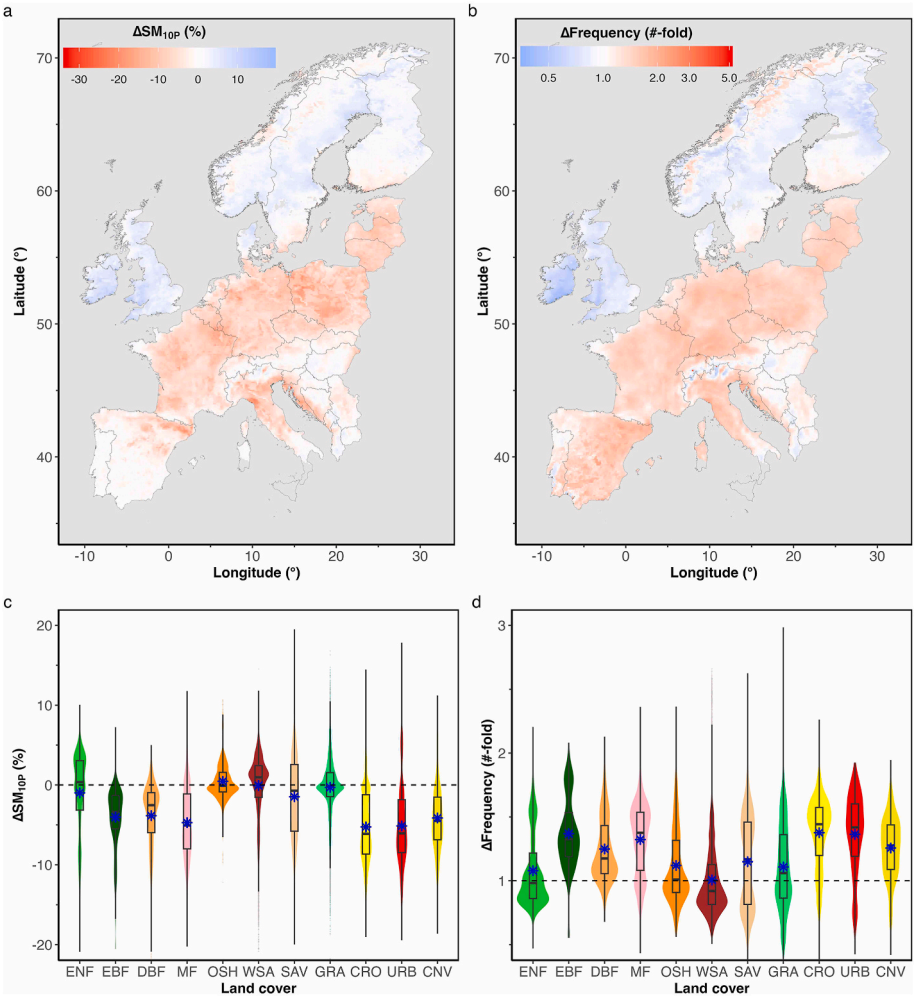

Fig. 2. Change in intensity (as indicated by SM_{10P}) (a, c) and frequency (b, d) of extreme soil dryness across Europe and land cover types (as violin plots indicating data distribution) during the present period (1991–2021) in comparison to the reference period (1950–1990). The change in intensity is calculated as % change in the present period compared to the reference period of SM_{10P} (10^{th} percentile of SM) indicated as ΔSM_{10P} (100 × (present–reference)/reference). The change in frequency of occurrences (ΔFrequency) is shown in terms of n-fold (present/reference). The blue asterisks in c and d shows the means. The land cover types were based on the IGBP land cover classification (see Methods or caption of Fig. S1). (For interpretation of the references to colour in this figure legend, the reader is referred to the Web version of this article.)

strength of SM-VPD coupling during the present period was highest in NEU and the Alpine region of CEU (Fig. 4a). Furthermore, overall, the daily SM-VPD coupling was significantly lower than monthly SM-VPD coupling (Fig. S4a) as also observed in previous studies but there were regional differences.

To quantify the impact on daily SM-VPD coupling on the frequency of occurrence of extreme compound dryness, we calculated the probability multiplication factor (PMF). The PMF indicated the increased probability (or frequency of occurrence) of extreme compound dryness compared to that expected when SM and VPD are independent (i.e., $P = 0.1 \times 0.1 = 0.01$; see Methods). The PMF across Europe during the reference period was 3.6 [2.5, 4.2] (median [10^{th} percentile, 90^{th} percentile]), indicating that the frequency of co-occurrence of soil and air dryness (i.e., extreme compound dryness) during the reference period was 3.6 time more than if SM and VPD would have been independent (Fig. S5a). As expected, due to increased SM-VPD coupling over large parts of Europe (Fig. 4), the PMF during the present period increased to 4 [2.9, 4.6] across Europe (Fig. S5b). This increase in present day PMF compared to the reference PMF was largest over NEU, Alpine region, and southern Spain (more than 1.5-fold; Fig. 5a). However, across France and southern Italy, the PMF decreased during the present period (Fig. 5a). Among different land cover types, the highest observed increase in PMF was over shrublands and grasslands (mean of 1.2-fold; Fig. 5b). The relationship between daily SM and VPD coupling, as indicated by r (SM, VPD), and PMF for extreme compound dryness was largely linear, with an increase of PMF with increase in negative coupling in CEU and NEU (Fig. 6). However, in MED, we observed a decrease in PMF for r (SM, VPD) < -0.6 as shown in Fig. 6. Furthermore, the relationship between PMF and r (SM, VPD) was significantly different between reference and present period over MED (for r (SM, VPD) < -0.6) and NEU (for r (SM, VPD) < -0.2), with higher PMF values during the present period compared to reference period (Fig. 6). However, across CEU, the PMF vs r (SM, VPD) relationship remained unchanged during present and reference period (Fig. 6). Additionally, similar to the SM-VPD coupling, overall, the PMF at daily timescale was significantly lower than PMF at monthly timescale (Fig. S4b), indicating overestimation of frequency of compound extreme dryness at monthly timescales in comparison to daily timescales.

3.4. Change in frequency of extreme compound dryness

The probability of the occurrence, which indicates frequency, of extreme compound dryness (P_{CD}) across Europe during the reference period is also equal to the PMF of the reference period, i.e., 3.5 ± 0.7 %

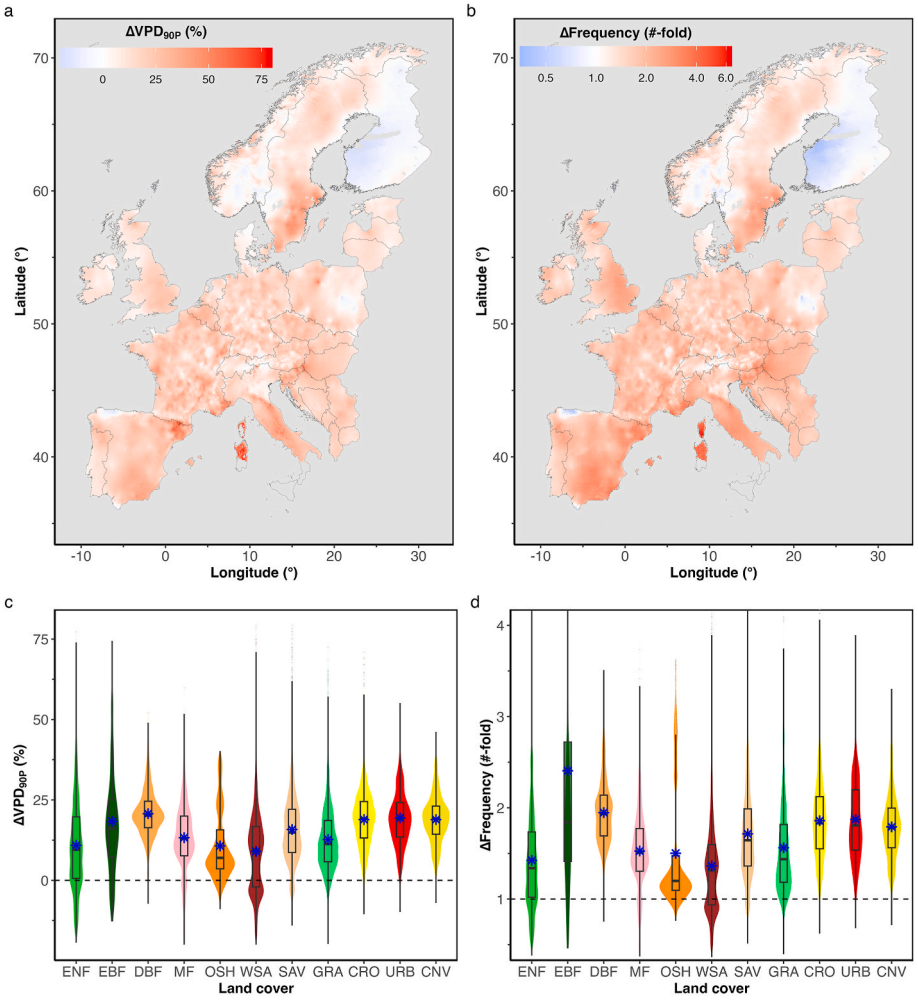

Fig. 3. Change in intensity (as indicated by VPD_{90P}) (a, c) and frequency (b, d) of extreme air dryness across Europe and land cover types (as violin plots indicating data distribution) during the present period (1991–2021) in comparison to the reference period (1950–1990). The change in intensity is calculated as % change in the present period compared to the reference period of VPD_{90P} (90^{th} percentile of VPD) indicated as ΔVPD_{90P} (100 × (present–reference)/reference). The change in frequency of occurrences (ΔFrequency) is shown in terms of n-fold (present/reference). The blue asterisks in c and d shows the means. The land cover types were based on the IGBP land cover classification (see Methods or caption of Fig. S1). (For interpretation of the references to colour in this figure legend, the reader is referred to the Web version of this article.)

(mean ± sd) as shown in Fig. 7a. Using the SM_{10P} and VPD_{90P} thresholds from the reference period, the P_{CD} increased to 6.0 ± 2.4% during the present period (Fig. 7b), thereby showing a 1.7-fold [0.9,2.5] (median [10^{th}, 90^{th} percentile]) increase overall across Europe and more than two-fold increase for more than one-quarter of the European land area (Fig. 7c). The increase in P_{CD} was highest in the MED (more than four-fold increase), whereas a decrease in occurrence was observed in some areas of NEU (i.e., Finland, Ireland, and the western part of the UK), comprising about 12% of the study area (Fig. 7c). To understand if this increase in P_{CD} was due to increase in SM-VPD coupling or due to decreasing SM and/or increasing VPD trend from reference to present period, we calculated ΔP_{CD} due to SM-VPD coupling (ratio of PMF in present and reference period) and due to SM and VPD trend (ratio of P_{CD} and PMF of reference period; see Methods). Our results indicate that the increase in P_{CD} across CEU (excluding the Alpine area) and MED was dominantly due to the decreasing SM and/or increasing VPD trend from reference to the present period (Fig. 8a). Whereas, for much of the NEU and Alpine region in CEU, the ΔP_{CD} was due to the increased SM-VPD coupling from reference to the present period. Overall, the change in SM-VPD coupling (as shown in Figs. 4 and 5) resulted in a ΔP_{CD} of 1.1-fold [0.9,1.4], whereas decreasing SM and/or increasing VPD trend resulted in a ΔP_{CD} of 1.5-fold [0.9, 2.3] (Figs. S6 and 8b). Among different land cover types, we observed a mean increase in the frequency by more than two-fold over evergreen broadleaved forests, croplands, and urban areas during the present period in comparison to the reference period (Fig. 7d).

3.5. *Future projections of extreme compound dryness*

Climate projections indicated a further compound drying (both soil and air drying) trend across Europe. Compared to the reference period, the decrease in average SM_{10P} across Europe was only marginal, i.e., 1%, 3% and 3.5% decrease during the present period, the mid 21^{st} century (2031–2065), and the late 21^{st} century (2066–2100), respectively (Fig. S7a) with largest decrease across MED (Fig. S8a). The VPD_{90P} however showed an average increase across Europe by 13%, 33% and 65% compared to the reference period, during the present period, the mid 21^{st} century, and the late 21^{st} century, respectively, as simulated by the 12 RCMs (Fig. S7b), with largest increase in CEU (Fig. S8b). Furthermore, the ensemble means value (mean from all 12 RCMs) of the Pearson coefficient correlation – r (SM, VPD) indicated a significantly increasing SM-VPD coupling from 1950 to 2100 (larger negative correlations from reference to future periods; Fig. S9). The RCM models, however, underestimated the SM-VPD coupling as the mean correlation

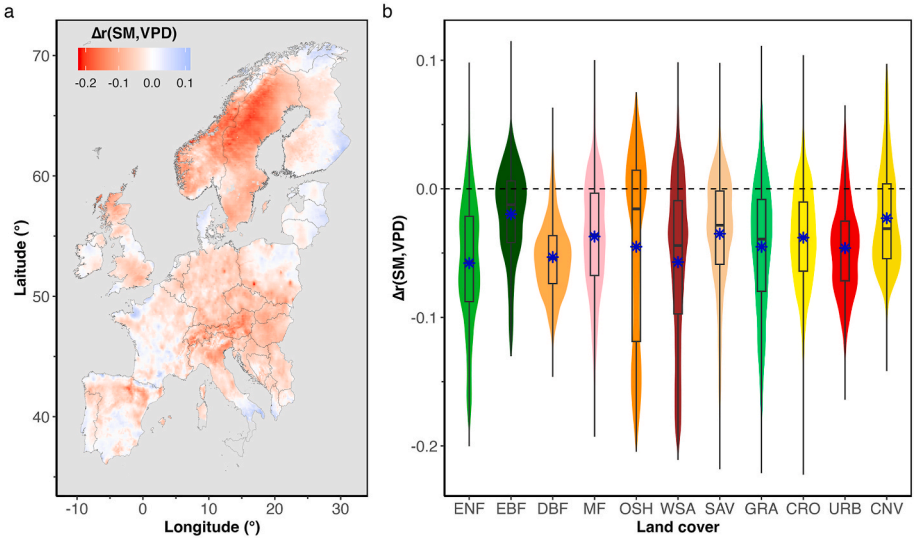

Fig. 4. Change in negative coupling (present-reference) between daily topsoil SM and VPD as indicated by change in Pearson correlation coefficient [Δr (SM,VPD)] between present and reference period (a) across Europe and (b) land cover types (as violin plots indicating data distribution). The blue asterisk in b shows the means. The land cover types were based on the IGBP land cover classification (see Methods or caption of Fig. S1). (For interpretation of the references to colour in this figure legend, the reader is referred to the Web version of this article.)

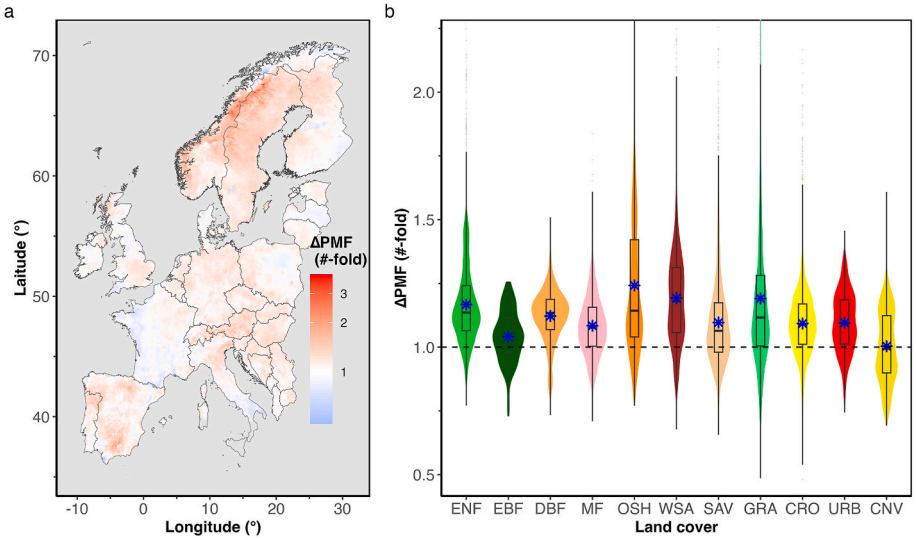

Fig. 5. Change in probability multiplication factor (PMF) of extreme compound dryness during as (a) number of fold (ΔPMF; present/reference) across Europe and its (b) segregation across different land cover types (as violin plots indicating data distribution). The blue asterisk in panel d shows the means. The land cover types are based on the IGBP land cover classification (see Methods or caption of Fig. S1). (For interpretation of the references to colour in this figure legend, the reader is referred to the Web version of this article.)

coefficient during reference and present period obtained from RCM models were −0.32 and −0.34 (Fig. S9), significantly lower than the correlation coefficient obtained from E-OBS and ERA5-Land data (−0.56 and −0.63 during reference and present periods, respectively as shown in Fig. S3). Furthermore, the increase in SM-VPD coupling simulated by the RCMs did not significantly increase the PMF of extreme compound dryness across MED, CEU, and NEU (Fig. S10).

Owing to the underestimation of the SM-VPD coupling in the RCM models, the P_{CD} was also lower (2 ± 0.8% (mean ± sd) and 3.7 ± 2% during reference and present periods, respectively; Fig. S11a) than what was calculated based on the in-situ and reanalysis data (E-OBS and ERA5-Land) with 3.5 ± 0.7 % and 6.0 ± 2.4% during reference and present period, respectively (Fig. S6). However, no significant change was observed in P_{CD} during the present period in comparison to the reference period, obtained by in-situ and reanalysis data (E-OBS and ERA5-Land), and the 12 RCM ensembles i.e., 1.72-fold [0.94, 2.51] (median [10th percentile, 90th percentile] increase from the former dataset and 1.74-fold [1.05, 2.57] increase from latter dataset (Fig. S11b). This pattern was also spatially consistent across different land cover types (Fig. S11c).

For the future, the RCM ensembles showed a 3.3-fold [2, 5.8] (median [10th percentile, 90th percentile]) increase in the frequency of extreme compound dryness across Europe during the mid 21st century (2031–2065 period) compared to reference period (Fig. S11b) with the largest increase in MED, some parts of NEU (high latitudes of Norway, Sweden, and Finland) and the surrounding Alpine region in CEU (Fig. 9a). All land cover types are projected to experience on average more than three times the frequency of extreme compound dryness by the mid 21st century as compared to the reference period, with the highest increase in frequency for open shrublands (Fig. 9c). By the late

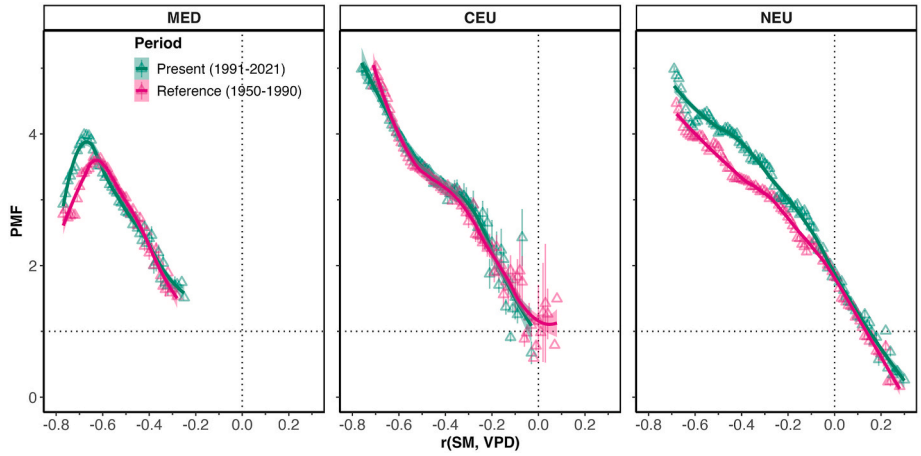

Fig. 6. Relationship of coefficient correlation between daily SM and VPD (x-axis: r (SM,VPD) with probability multiplication factor of extreme compound dryness across Mediterranean Europe (MED), Central Europe (CEU) and Northern Europe (NEU) during reference period (1950–1990) and present period (1991–2021). The curve fitting is done with a locally moving weighted regression (loess with span = 0.8). Each point and error bar represents mean and standard error for a bin of r (SM,VPD) = 0.01.

21st century (2066–2100), the projections indicated a further increase in the frequency of occurrence of extreme compound dryness of 4.6-fold [2.3, 11.9] in comparison to the reference period (Fig. S11b), with a spatial pattern rather similar to that of the mid 21st century (Fig. 9b). Only the northern part of CEU (northern Germany and Poland) indicated a decreased frequency of extreme compound dryness during the late 21st century in comparison to mid 21st century, most likely due to an increase in SM_{10P} (Fig. S8a). Among different land cover types, open shrublands, grasslands and broadleaved forests were projected to experience more than five times more frequent extreme compound dryness during the late 21st century compared to the late 20th century (Fig. 9d). Finally, the increase in frequency of extreme compound dryness during mid 21st century and late 21st century compared to the reference period is entirely and dominantly driven by decreasing SM and/or increasing VPD trend from reference to future periods throughout Europe.

4. Discussion

Here, we assessed the past (1950–2021) and future (up to 2100) evolution of the frequency and intensity of extreme soil dryness and/or extreme air dryness across Europe at a higher spatio-temporal resolution (0.1° × 0.1°, and daily). Our study showed that large parts of Europe, especially Central and Mediterranean Europe, have been experiencing increasing trends in model-based soil moisture and observation-based atmospheric drying, thereby resulting in the development of compound dry conditions since 1950. We showed that compared to the reference period (1950–1990), the frequency of extreme compound dryness, extreme soil dryness and extreme air dryness across Europe during 1991–2021 increased by a median of 1.7-fold, 1.2-fold, and 1.6-fold, respectively, mostly over Central and Mediterranean Europe. We hypothesized that - the increase in frequency and intensity of extreme compound dryness would be largely due to increased SM-VPD coupling across Europe, was only true for Northern Europe, as increasing trend in soil and air drying resulted in increased compound extreme across Central and Mediterranean Europe from 1990 to 2021 compared to the reference period. Regional climate model simulations for Europe indicated a further 3.3-fold (median) increase in the frequency of compound dry extremes during mid-century (2031–2065), and a 4.6-fold increase during the late 21st century (2066–2100), most pronounced over present day broadleaved forests, croplands, and urban areas.

Our study builds on a previous study (Zhou et al., 2019b) which highlighted the increase in frequency of compound air and soil dryness globally using data from earth system models (ESMs) at monthly timescale. The change in probability multiplication factor (PMF) obtained at a monthly scale was larger than that at daily scale (Fig. S4), indicating substantial overestimation of frequency of extreme compound dryness. It is known that carbon and water fluxes of terrestrial ecosystems shows immediate response to variation in weather, particularly at daily time scales. Daily ecosystem-level gas exchange observations (e.g., by the eddy covariance method) have shown how rapidly ecosystems respond to climate extremes and over short timescales (Geddes et al., 2014; Gou et al., 2023, 2024; Shekhar et al., 2024; Stoy et al., 2009; Tatarinov et al., 2016; Yuan et al., 2016; Zhou et al., 2021). Furthermore, high-resolution tree growth measurements collected with dendrometers show that extreme atmospheric dryness and low soil moisture conditions affect tree growth on the daily and even sub-daily time scale (Zweifel et al., 2021). Therefore, our results highlighted here are of high relevance for assessing the future exposure of extreme dryness on European ecosystems and future food security (Shekhar and Shapiro, 2022). Furthermore, the high spatial resolution of our analysis enabled us to segregate the increase in extremes, across present land cover types and regions (e.g., Alpine, Mediterranean, Northern Europe) across Europe. Our study showed that large parts of Europe, especially Central and Mediterranean Europe, have been experiencing increasing trends in model-based soil moisture and observation-based atmospheric drying, thereby resulting in the development of compound dry conditions since 1950.

The lower RCM based increase in frequency and intensity of extreme soil dryness than that from ERA5-Land was probably due to a disagreement in SM depth i.e., surface SM (0–7 cm) from ERA-Land, whereas that from the RCM represents the soil moisture over the complete soil profile (depth varying from 2.7 m to 3 m), as surface and total soil moisture trends as simulated by RCMs could different (Berg et al., 2017). The changes in extreme air dryness (relative to the reference period) as simulated by the RCMs agreed well with the observations across Europe. The RCMs showed a weaker daily SM and VPD coupling than that from the reanalysis/observation datasets, contradicting the results (Levine et al., 2016; Ukkola et al., 2016) that suggested a stronger SM and VPD coupling than the observations in GCMs. However, the higher SM and VPD correlations from the reanalysis/observation datasets could be a result from the different soil depth considered, as fluctuations of surface soil moisture is higher than a complete soil profile. Nevertheless, both RCM data for RCP8.5 projection and reanalysis/observation data showed similar change in occurrence probability of extreme compound dryness (74% for the former and 72% for the latter) during the present period compared to reference period. This indicated that the potential bias (in absolute values) between the RCMs and the reanalysis/observation data seemed to have little effect on the

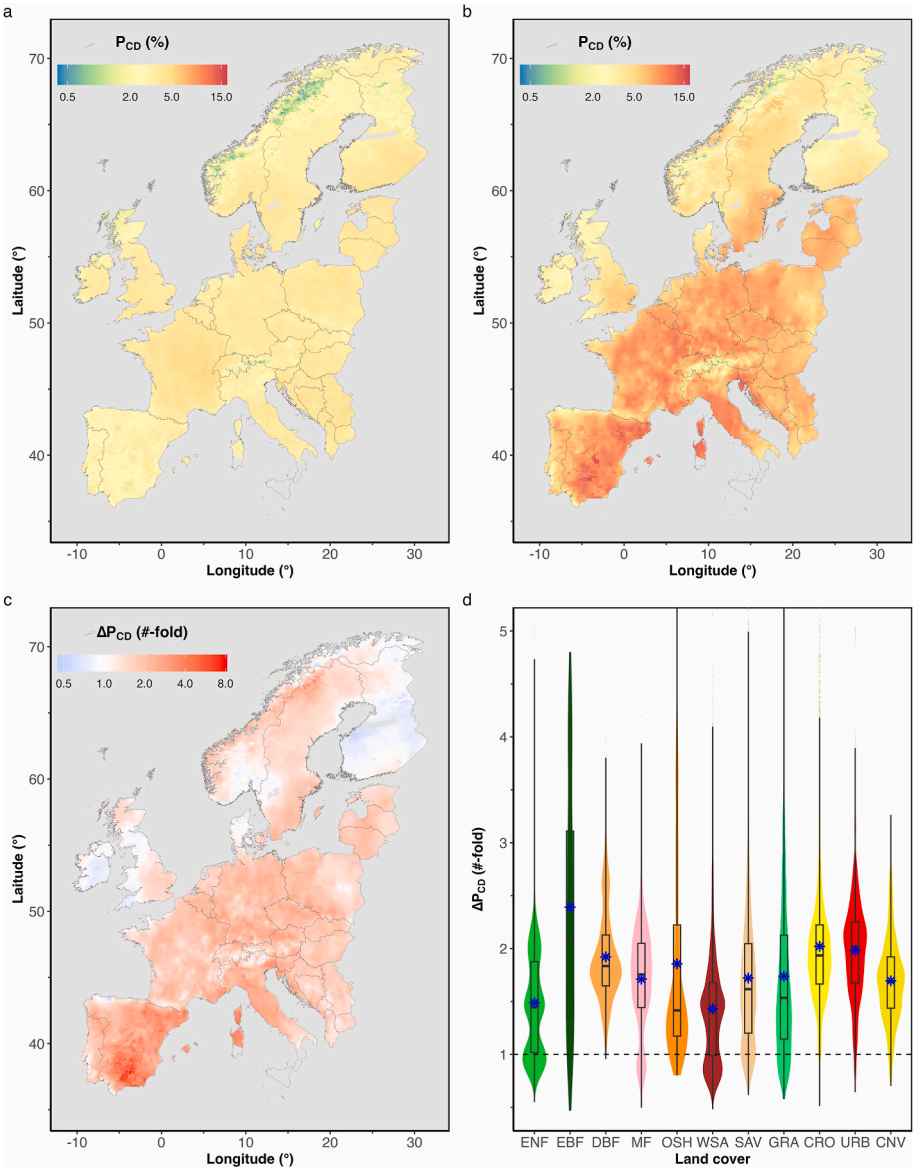

Fig. 7. Probability of the occurrence indicating frequency of extreme compound dryness (P_{CD}) during (a) the reference period, (b) the present period (with SM and VPD thresholds from reference period), (c) change in probability of extreme compound dryness (ΔP_{CD}) between present and reference period (ΔP_{CD} = present/reference), and (d) the change across different land cover types (as violin plots indicating data distribution). The blue asterisk in panel d shows the means. The land cover types are based on the IGBP land cover classification (see Methods or caption of Fig. S1). (For interpretation of the references to colour in this figure legend, the reader is referred to the Web version of this article.)

relative change in SM and VPD coupling over time. This observation was similar to recent studies showing RCMs and observation based agreement on warming trends even though there is substantial air temperature bias between RCMs and observations (Kotlarski et al., 2014; van der Wiel et al., 2020). A similar analysis with RCP4.5 projection data (not shown) indicated a significant underestimation (55% increase in occurrence probability of extreme compound dryness during the present period compared to reference period) compared to the observational dataset, thus not included in this study.

The increase in the frequency and intensity of compound dry extremes over time was generally due to two reasons, first due to an increased negative coupling between SM and VPD, and second due to an increasing trend of VPD and/or decreasing trend of SM, both signs of increasing dryness. The increase in the negative SM-VPD coupling (during 1991–2021 compared to the reference period) was a major reason of the increased frequency of extreme compound dryness across NEU, whereas the increased frequency of extreme compound dryness for much of CEU and MED was due to both above mentioned reasons but dominantly due to increasing trend of VPD and/or decreasing trend of SM. Such a SM-VPD coupling-driven increase and trend-driven increase in frequency of compound hot and drought events in Europe was also reported earlier (Cardell et al., 2020; Markonis et al., 2021). However, we observed that much of the increased frequency and intensity of extreme compound dryness in future was due to increased air dryness across Europe. A similar study (Zhou et al., 2019b) using GCM simulations, also highlighted that the increase in frequency probability of extreme compound dryness (at a monthly timescale) was largely due to an increasing trend of VPD in the future.

The extreme compound dryness is a result of a series of complementary physical processes involving land-atmosphere feedbacks. High VPD-driven increases in ET reduces SM which then reduces ET and thus increases the sensible heat flux which warms and dries near-surface air, thereby increasing VPD, ultimately creating a positive feedback loop (Gentine et al., 2013; Miralles et al., 2019; Seneviratne et al., 2013;

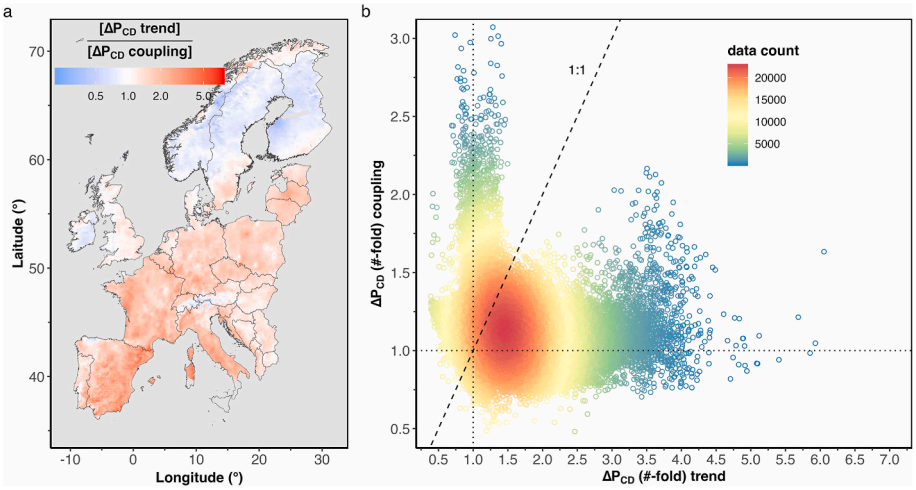

Fig. 8. (a) Ratio of change in probability of occurrence of extreme compound dryness between present and reference period (ΔP_{CD} = present/reference) due to SM and VPD trend and SM-VPD coupling across Europe and (b) comparison of the ΔP_{CD} due to trend of SM and VPD (x-axis) and SM-VPD coupling (y-axis) for all locations in Europe. Values lower than one in panel a and above the 1:1 line in panel b indicate that SM-VPD coupling was the dominant reason for ΔP_{CD}, whereas values greater than one in panel a and below the 1:1 line in panel b indicate that the ΔP_{CD} was dominantly due to the trend of SM and VPD.

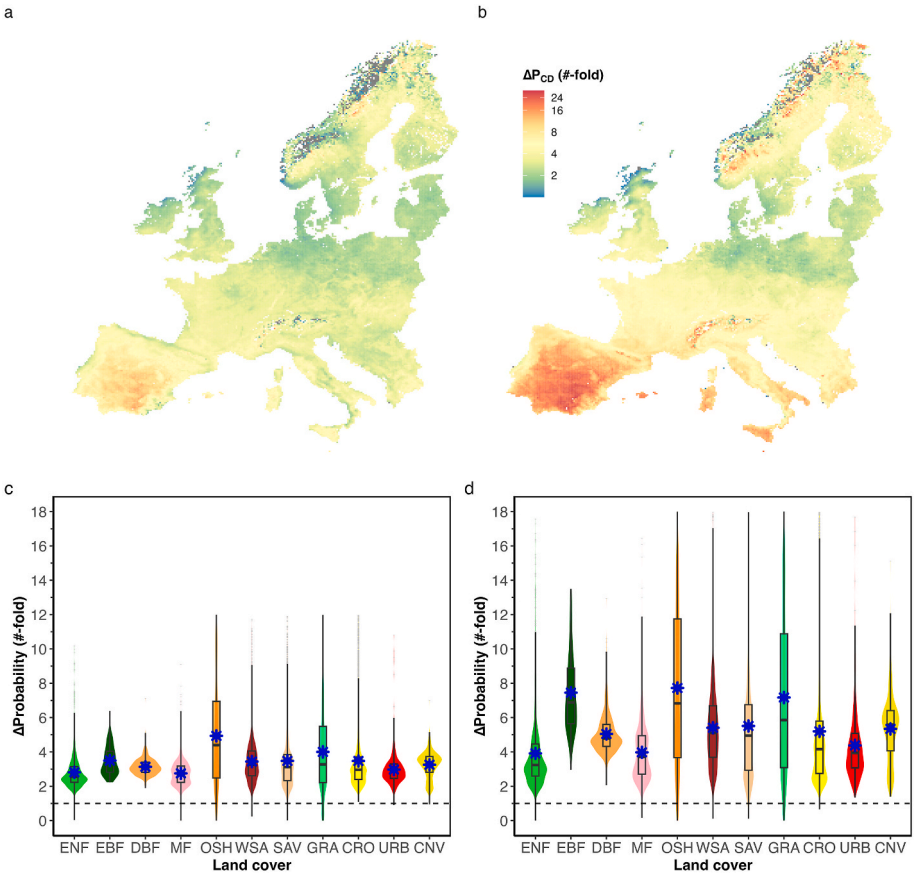

Fig. 9. Change in probability of extreme compound dryness compared to the reference period (1950–1990) across Europe during (a) mid 21st century (2031–2065) and (b) late 21st century and across different land cover types (as violin plots indicating data distribution) during (c) mid 21st century and (d) late 21st century. The blue asterisk in panels c and d shows the means. The land cover types are based on the IGBP land cover classification (see Fig. S1). (For interpretation of the references to colour in this figure legend, the reader is referred to the Web version of this article.)

Shekhar et al., 2023; Sippel et al., 2018; Zhou et al., 2019a). These feedback loops are much stronger over semi-arid regions than humid regions (Miralles et al., 2019), which also explains the largest increase in the frequency of compound extreme in the present and the future over majority of Mediterranean Europe. Apart from these feedback loops, large-scale atmospheric anomalies such as blocking, subsidence, and free tropospheric warming had been identified as key contributors to the onset and continuation of extreme compound dry conditions (Fang et al., 2022; Pfahl et al., 2015). These anomalies might also have contributed to the SM-VPD interaction.

The increasing trend in VPD was largely due to global warming driven-increase in air temperature, whereas soil drying trends could be due to increased ET trends in Europe with non-significant precipitation change over the last 40 years (Fang et al., 2022; He et al., 2022; Lal et al., 2023). Furthermore, the future projections of intensifying VPD and drying SM along with the increase in negative coupling between SM-VPD could further increase the frequency and intensity of compound dry extremes in Europe. Owing to the direct role of SM and VPD on vegetation productivity, the future carbon uptake capacity could be highly compromised due to the rise in dry extremes in Europe. Although it is possible that future CO_2 fertilization effects (increased gross primary productivity due to more CO_2 rich atmosphere) could compensate for the loss in carbon uptake caused by extreme compound dryness (Campbell et al., 2017), the ESM (Earth System Models) forecasts showed that this was not the case for Central and Mediterranean Europe, but for Northern Europe (Zhou et al., 2019b), resulting in an unchanged future CO_2 uptake.

5. Conclusions

Our study detected extreme dryness across Europe at a higher spatio-temporal (0.1° and daily) resolution than previous studies which were conducted based on GCM and ESM simulations of much coarser resolution (e.g., 2.5° and monthly). At this higher resolution, we were able to segregate the changes in frequency of extreme dryness across the most recent (year 2021) land cover types in Europe, to quantify their present and future exposure to extreme dryness. This segregation is important for future climate mitigation planning and development of nature based solutions to our climate issues. Although almost all the land cover types were exposed to increased frequency of extreme dryness (all three types), croplands, broadleaved forest (EBF and DBF) and urban areas experienced more than twice as much extreme dryness conditions during 1990–2021 compared to reference period of 1990–2021. In the future, these land cover types would be exposed to more than three times as many extremes during mid-21st century compared to the 1950–1990 period. Such a high increase in extremes exposure will increase their vulnerability in the future, leading to a weaker terrestrial carbon sink and compromised food security across Europe. The prominent pattern of extreme dryness shown here is an essential first step in understanding how compound dryness has evolved over the years, and in developing new adaptive management policies to reduce the risks of upcoming hydroclimatic hazards.

Data and code availability

All data used in this study is openly available in the following database. The E-OBS and ERA5-Land datasets were downloaded from the climate data store of Copernicus Climate Change Service (https://cds.climate.copernicus.eu). The 2021 MODIS land cover product MCD12Q1 Version 6.1 was downloaded from USGS LP DAAC website https://lpdaac.usgs.gov/products/mcd12c1v061/. The EURO-CORDEX simulations were downloaded from ESGF data node https://esgf-data.dkrz.de/search/cordex-dkrz/. All data and R script used to construct the visuals in the manuscript can be requested from the corresponding author.

CRediT authorship contribution statement

Ankit Shekhar: Conceptualization, Data curation, Formal analysis, Investigation, Methodology, Software, Validation, Visualization, Writing – original draft. **Nina Buchmann:** Funding acquisition, Project administration, Supervision, Writing – review & editing. **Vincent Humphrey:** Conceptualization, Methodology, Writing – review & editing. **Mana Gharun:** Conceptualization, Funding acquisition, Methodology, Project administration, Supervision, Writing – review & editing.

Declaration of competing interest

The authors declare that they have no known competing financial interests or personal relationships that could have appeared to influence the work reported in this paper.

Data availability

All data used in this study is openly available and the links are provided in the manuscript.

Acknowledgement

The authors are grateful to Climate Data Store (CDS) and Earth System Grid Federation (ESGF) for freely providing the data used in this study. The authors acknowledge funding from the ETH Zürich project FEVER (ETH-27 19-1) and SNF funded project EcoDrive (IZCOZ0_198094). The authors also acknowledge valuable feedback from two anonymous reviewer during the review process. The APC funding from ETH-Bibliothek is highly acknowledged.

Appendix A. Supplementary data

Supplementary data to this article can be found online at https://doi.org/10.1016/j.wace.2024.100666.

References

Albergel, C., De Rosnay, P., Balsamo, G., Isaksen, L., Muñoz-Sabater, J., 2012. Soil moisture analyses at ECMWF: evaluation using global ground-based in situ observations. J. Hydrometeorol. 13, 1442–1460. https://doi.org/10.1175/JHM-D-11-0107.1.

Bastos, A., Orth, R., Reichstein, M., Ciais, P., Viovy, N., Zaehle, S., Anthoni, P., Arneth, A., Gentine, P., Joetzjer, E., Lienert, S., Loughran, T., McGuire, P.C., O, S., Pongratz, J., Sitch, S., 2021. Vulnerability of European ecosystems to two compound dry and hot summers in 2018 and 2019. Earth Syst. Dyn. 12, 1015–1035. https://doi.org/10.5194/esd-12-1015-2021.

Berg, A., Sheffield, J., Milly, P.C.D., 2017. Divergent surface and total soil moisture projections under global warming. Geophys. Res. Lett. 44, 236–244. https://doi.org/10.1002/2016GL071921.

Campbell, J.E., Berry, J.A., Seibt, U., Smith, S.J., Montzka, S.A., Launois, T., Belviso, S., Bopp, L., Laine, M., 2017. Large historical growth in global terrestrial gross primary production. Nature 544, 84–87. https://doi.org/10.1038/nature22030.

Cardell, M.F., Amengual, A., Romero, R., Ramis, C., 2020. Future extremes of temperature and precipitation in Europe derived from a combination of dynamical and statistical approaches. Int. J. Climatol. 40, 4800–4827. https://doi.org/10.1002/JOC.6490.

Cornes, R.C., van der Schrier, G., van den Besselaar, E.J.M., Jones, P.D., 2018. An ensemble version of the E-OBS temperature and precipitation data sets. J. Geophys. Res. Atmos. 123, 9391–9409. https://doi.org/10.1029/2017JD028200.

Fang, Z., Zhang, W., Brandt, M., Abdi, A.M., Fensholt, R., 2022. Globally increasing atmospheric aridity over the 21st century. Earth's Future 10, e2022EF003019. https://doi.org/10.1029/2022EF003019.

Friedl, M., Sulla-Menashe, D., 2015. MCD12C1 MODIS/Terra+ aqua land cover type yearly L3 global 0.05 Deg CMG V006 [data set]. NASA EOSDIS land process. DAAC. https://doi.org/10.5067/MODIS/MCD12C1.006.

Fu, Z., Ciais, P., Prentice, I.C., Gentine, P., Makowski, D., Bastos, A., Luo, X., Green, J.K., Stoy, P.C., Yang, H., Hajima, T., 2022. Atmospheric dryness reduces photosynthesis along a large range of soil water deficits. Nat. Commun. 2022 (131 13), 1–10. https://doi.org/10.1038/s41467-022-28652-7.

Geddes, J.A., Murphy, J.G., Schurman, J., Petroff, A., Thomas, S.C., 2014. Net ecosystem exchange of an uneven-aged managed forest in central Ontario, and the impact of a spring heat wave event. Agric. For. Meteorol. 198–199, 105–115. https://doi.org/10.1016/j.agrformet.2014.08.008.

Genest, C., Favre, A.-C., 2007. Everything you always wanted to know about copula modeling but were afraid to ask. J. Hydrol. Eng. 12, 347–368. https://doi.org/10.1061/(ASCE)1084-0699(2007)12:4(347).

Gentine, P., Holtslag, A.A.M., D'Andrea, F., Ek, M., 2013. Surface and atmospheric controls on the onset of moist convection over land. J. Hydrometeorol. 14, 1443–1462. https://doi.org/10.1175/JHM-D-12-0137.1.

Gou, R., Buchmann, N., Chi, J., Luo, Y., Mo, L., Shekhar, A., Feigenwinter, I., Hörtnagl, L., Lu, W., Cui, X., Meng, Y., Song, S., Lin, Guangxuan, Chen, Y., Liang, J., Guo, J., Peng, H., Lin, Guanghui, 2023. Temporal variations of carbon and water fluxes in a subtropical mangrove forest: insights from a decade-long eddy covariance measurement. Agric. For. Meteorol. 343, 109764 https://doi.org/10.1016/j.agrformet.2023.109764.

Gou, R., Chi, J., Liu, J., Luo, Y., Shekhar, A., Mo, L., Lin, G., 2024. Atmospheric water demand constrains net ecosystem production in subtropical mangrove forests. J. Hydrol. 630, 130651 https://doi.org/10.1016/j.jhydrol.2024.130651.

He, B., Chen, C., Lin, S., Yuan, W., Chen, H.W., Chen, D., Zhang, Y., Guo, L., Zhao, X., Liu, X., Piao, S., Zhong, Z., Wang, R., Tang, R., 2022. Worldwide impacts of atmospheric vapor pressure deficit on the interannual variability of terrestrial carbon sinks. Natl. Sci. Rev. 9 https://doi.org/10.1093/NSR/NWAB150.

Hermann, M., Röthlisberger, M., Gessler, A., Rigling, A., Senf, C., Wohlgemuth, T., Wernli, H., 2023. Meteorological history of low-forest-greenness events in Europe in 2002–2022. Biogeosciences 20, 1155–1180. https://doi.org/10.5194/bg-20-1155-2023.

Hersbach, H., Bell, B., Berrisford, P., Hirahara, S., Horányi, A., Muñoz-Sabater, J., Nicolas, J., Peubey, C., Radu, R., Schepers, D., Simmons, A., Soci, C., Abdalla, S., Abellan, X., Balsamo, G., Bechtold, P., Biavati, G., Bidlot, J., Bonavita, M., Chiara, G., Dahlgren, P., Dee, D., Diamantakis, M., Dragani, R., Flemming, J., Forbes, R., Fuentes, M., Geer, A., Haimberger, L., Healy, S., Hogan, R.J., Hólm, E., Janisková, M., Keeley, S., Laloyaux, P., Lopez, P., Lupu, C., Radnoti, G., Rosnay, P., Rozum, I., Vamborg, F., Villaume, S., Thépaut, J., 2020. The ERA5 global reanalysis. Q. J. R. Meteorol. Soc. 146, 1999–2049. https://doi.org/10.1002/qj.3803.

Hijmans, R.J., Etten, J. van, Mattiuzzi, M., Sumner, M., Greenberg, J.A., Lamigueiro, O. P., Bevan, A., Racine, E.B., Shortridge, A., 2014. Package "raster.". R.

Humphrey, V., Berg, A., Ciais, P., Gentine, P., Jung, M., Reichstein, M., Seneviratne, S.I., Frankenberg, C., 2021. Soil moisture-atmosphere feedback dominates land carbon uptake variability. Nature 592, 65–69. https://doi.org/10.1038/s41586-021-03325-5.

Ionita, M., Tallaksen, L.M., Kingston, D.G., Stagge, J.H., Laaha, G., Van Lanen, H.A.J., Scholz, P., Chelcea, S.M., Haslinger, K., 2017. The European 2015 drought from a climatological perspective. Hydrol. Earth Syst. Sci. 21, 1397–1419. https://doi.org/10.5194/hess-21-1397-2017.

Jones, Hamlyn G., 2014. Plants and Microclimate: A Quantitative Approach to Environmental Plant Physiology, third ed. Cambridge University Press.

Klein Tank, A.M.G., Wijngaard, J.B., Können, G.P., Böhm, R., Demarée, G., Gocheva, A., Mileta, M., Pashiardis, S., Hejkrlik, L., Kern-Hansen, C., Heino, R., Bessemoulin, P., Müller-Westermeier, G., Tzanakou, M., Szalai, S., Pálsdóttir, T., Fitzgerald, D., Rubin, S., Capaldo, M., Maugeri, M., Leitass, A., Bukantis, A., Aberfeld, R., van Engelen, A.F.V., Forland, E., Mietus, M., Coelho, F., Mares, C., Razuvaev, V., Nieplova, E., Cegnar, T., Antonio López, J., Dahlström, B., Moberg, A., Kirchhofer, W., Ceylan, A., Pachaliuk, O., Alexander, L.V., Petrovic, P., 2002. Daily dataset of 20th-century surface air temperature and precipitation series for the European Climate Assessment. Int. J. Climatol. 22, 1441–1453. https://doi.org/10.1002/joc.773.

Kong, D., Song, H., 2022. Rtrend: trend estimating tools. R Package Version 013.

Kotlarski, S., Keuler, K., Christensen, O.B., Colette, A., Déqué, M., Gobiet, A., Goergen, K., Jacob, D., Lüthi, D., van Meijgaard, E., Nikulin, G., Schär, C., Teichmann, C., Vautard, R., Warrach-Sagi, K., Wulfmeyer, V., 2014. Regional climate modeling on European scales: a joint standard evaluation of the EURO-CORDEX RCM ensemble. Geosci. Model Dev. (GMD) 7, 1297–1333. https://doi.org/10.5194/gmd-7-1297-2014.

Lal, P., Shekhar, A., Gharun, M., Das, N.N., 2023. Spatiotemporal evolution of global long-term patterns of soil moisture. Sci. Total Environ. 867, 161470 https://doi.org/10.1016/j.scitotenv.2023.161470.

Lal, P., Singh, G., Das, N.N., Colliander, A., Entekhabi, D., 2022. Assessment of ERA5-land volumetric soil water layer product using in situ and SMAP soil moisture observations. Geosci. Rem. Sens. Lett. IEEE 19, 1–5. https://doi.org/10.1109/LGRS.2022.3223985.

Levine, P.A., Randerson, J.T., Swenson, S.C., Lawrence, D.M., 2016. Evaluating the strength of the land–atmosphere moisture feedback in Earth system models using satellite observations. Hydrol. Earth Syst. Sci. 20, 4837–4856. https://doi.org/10.5194/hess-20-4837-2016.

Liu, L., Gudmundsson, L., Hauser, M., Qin, D., Li, S., Seneviratne, S.I., 2020. Soil moisture dominates dryness stress on ecosystem production globally. Nat. Commun. 11, 4892. https://doi.org/10.1038/s41467-020-18631-1.

Markonis, Y., Kumar, R., Hanel, M., Rakovec, O., Máca, P., AghaKouchak, A., 2021. The rise of compound warm-season droughts in Europe. Sci. Adv. 7 https://doi.org/10.1126/sciadv.abb9668.

Miralles, D.G., Gentine, P., Seneviratne, S.I., Teuling, A.J., 2019. Land–atmospheric feedbacks during droughts and heatwaves: state of the science and current challenges. Ann. N. Y. Acad. Sci. 1436, 19–35. https://doi.org/10.1111/NYAS.13912.

Miralles, D.G., Teuling, A.J., Van Heerwaarden, C.C., De Arellano, J.V.G., 2014. Mega-heatwave temperatures due to combined soil desiccation and atmospheric heat accumulation. Nat. Geosci. 7, 345–349. https://doi.org/10.1038/ngeo2141.

Molina, M.O., Sánchez, E., Gutiérrez, C., 2020. Future heat waves over the Mediterranean from an Euro-CORDEX regional climate model ensemble. Sci. Rep. 10, 8801. https://doi.org/10.1038/s41598-020-65663-0.

Muñoz-Sabater, J., Dutra, E., Agustí-Panareda, A., Albergel, C., Arduini, G., Balsamo, G., Boussetta, S., Choulga, M., Harrigan, S., Hersbach, H., Martens, B., Miralles, D.G., Piles, M., Rodríguez-Fernández, N.J., Zsoter, E., Buontempo, C., Thépaut, J.N., 2021. ERA5-Land: a state-of-the-art global reanalysis dataset for land applications. Earth Syst. Sci. Data 13, 4349–4383. https://doi.org/10.5194/essd-13-4349-2021.

Nagler, T., Schepsmeier, U., Stoeber, J., Brechmann, E.C., Graeler, B., Erhardt, T., 2022. VineCopula: Statistical Inference of Vine Copulas.

Novick, K.A., Ficklin, D.L., Stoy, P.C., Williams, C.A., Bohrer, G., Oishi, A.C., Papuga, S. A., Blanken, P.D., Noormets, A., Sulman, B.N., Scott, R.L., Wang, L., Phillips, R.P., 2016. The increasing importance of atmospheric demand for ecosystem water and carbon fluxes. Nat. Clim. Change 6, 1023–1027. https://doi.org/10.1038/nclimate3114.

Peters, W., Krol, M.C., Van Der Werf, G.R., Houweling, S., Jones, C.D., Hughes, J., Schaefer, K., Masarie, K.A., Jacobson, A.R., Miller, J.B., Cho, C.H., Ramonet, M., Schmidt, M., Ciattaglia, L., Apadula, F., Heltai, D., Meinhardt, F., Di Sarra, A.G., Piacentino, S., Sferlazzo, D., Aalto, T., Hatakka, J., Ström, J., Haszpra, L., Meijer, H. a.J., Van Der Laan, S., Neubert, R.E.M., Jordan, A., Rodó, X., Morguí, J.-A., Vermeulen, A.T., Popa, E., Rozanski, K., Zimnoch, M., Manning, A.C., Leuenberger, M., Uglietti, C., Dolman, A.J., Ciais, P., Heimann, M., Tans, P.P., 2010. Seven years of recent European net terrestrial carbon dioxide exchange constrained by atmospheric observations. Global Change Biol. 16, 1317–1337. https://doi.org/10.1111/j.1365-2486.2009.02078.x.

Pfahl, S., Schwierz, C., Croci-Maspoli, M., Grams, C.M., Wernli, H., 2015. Importance of latent heat release in ascending air streams for atmospheric blocking. Nat. Geosci. 8, 610–614. https://doi.org/10.1038/ngeo2487.

R Core Team, 2021. R lang, 2021. R core team. In: Environ. Stat. Comput. R Found. Stat. Comput. Vienna Austria URL Httpwww R-Proj. Org.

Samaniego, L., Thober, S., Kumar, R., Wanders, N., Rakovec, O., Pan, M., Zink, M., Sheffield, J., Wood, E.F., Marx, A., 2018. Anthropogenic warming exacerbates European soil moisture droughts. Nat. Clim. Change 8, 421–426. https://doi.org/10.1038/s41558-018-0138-5.

Scapucci, L., Shekhar, A., Aranda-Barranco, S., Bolshakova, A., Hörtnagl, L., Gharun, M., Buchmann, N.. Compound soil and atmospheric drought events and CO_2 fluxes of a mixed deciduous forest: Occurrence, impact, and temporal contribution of main drivers, EGUsphere [preprint]. https://doi.org/10.5194/egusphere-2024-459.

Schulzweida, U., 2022. CDO User Guide.

Schwalm, C.R., Glendon, S., Duffy, P.B., 2020. RCP8.5 tracks cumulative CO2 emissions. Proc. Natl. Acad. Sci. USA 117, 19656–19657. https://doi.org/10.1073/pnas.2007117117.

Seneviratne, S., Nicholls, N., Easterling, D., Goodess, C., Kanae, S., Kossin, J., Luo, Y., Marengo, J., McInnes, K., Rahimi, M., Reichstein, M., Sorteberg, A., Vera, C., Zhang, X., Alexander, L.V., Allen, S., Benito, G., Cavazos, T., Clague, J., Conway, D., Della-Marta, P.M., Gerber, M., Gong, S., Goswami, B.N., Hemer, M., Huggel, C., van den Hurk, B., Kharin, V.V., Kitoh, A., Klein Tank, A.M.G., Li, G., Mason, S.J., McGuire, W., van Oldenborgh, G.J., Orlowsky, B., Smith, S., Thiaw, W., Velegrakis, A., Yiou, P., Zhang, T., Zhou, T., Zwiers, F.W., 2012. Changes in climate extremes and their impacts on the natural physical environment. Intergov. Panel Clim. Change IPCC 109–230. https://doi.org/10.7916/d8-6nbt-s431.

Seneviratne, S.I., Wilhelm, M., Stanelle, T., van den Hurk, B., Hagemann, S., Berg, A., Cheruy, F., Higgins, M.E., Meier, A., Brovkin, V., Claussen, M., Ducharne, A., Dufresne, J.-L., Findell, K.L., Ghattas, J., Lawrence, D.M., Malyshev, S., Rummukainen, M., Smith, B., 2013. Impact of soil moisture-climate feedbacks on CMIP5 projections: first results from the GLACE-CMIP5 experiment. Geophys. Res. Lett. 40, 5212–5217. https://doi.org/10.1002/grl.50956.

Shekhar, A., Chen, J., Bhattacharjee, S., Buras, A., Castro, A.O., Zang, C.S., Rammig, A., 2020. Capturing the impact of the 2018 european drought and heat across different vegetation types using OCO-2 solar-induced fluorescence. Rem. Sens. 12 https://doi.org/10.3390/rs12193249.

Shekhar, A., Hörtnagl, L., Buchmann, N., Gharun, M., 2023. Long-term changes in forest response to extreme atmospheric dryness. Glob. Change Biol. n/a 1–18. https://doi.org/10.1111/gcb.16846.

Shekhar, A., Hörtnagl, L., Paul-Limoges, E., Etzold, S., Zweifel, R., Buchmann, N., Gharun, M., 2024. Contrasting impact of extreme soil and atmospheric dryness on the functioning of trees and forests. Sci. Total Environ. 916, 169931 https://doi.org/10.1016/j.scitotenv.2024.169931.

Shekhar, A., Shapiro, C.A., 2022. Prospective crop yield and income return based on a retrospective analysis of a long-term rainfed agriculture experiment in Nebraska. Agric. Syst. 198, 103384 https://doi.org/10.1016/j.agsy.2022.103384.

Sippel, S., Reichstein, M., Ma, X., Mahecha, M.D., Lange, H., Flach, M., Frank, D., 2018. Drought, heat, and the carbon cycle: a review. Curr. Clim. Change Rep. 4, 266–286. https://doi.org/10.1007/s40641-018-0103-4.

Stoy, P.C., Richardson, A.D., Baldocchi, D.D., Katul, G.G., Stanovick, J., Mahecha, M.D., Reichstein, M., Detto, M., Law, B.E., Wohlfahrt, G., Arriga, N., Campos, J., McCaughey, J.H., Montagnani, L., Paw U, K.T., Sevanto, S., Williams, M., 2009. Biosphere-atmosphere exchange of CO_2 in relation to climate: a cross-biome analysis across multiple time scales. Biogeosciences 6, 2297–2312. https://doi.org/10.5194/bg-6-2297-2009.

Tatarinov, F., Rotenberg, E., Maseyk, K., Ogée, J., Klein, T., Yakir, D., 2016. Resilience to seasonal heat wave episodes in a Mediterranean pine forest. New Phytol. 210, 485–496. https://doi.org/10.1111/NPH.13791.

Teuling, A.J., 2018. A hot future for European droughts. Nat. Clim. Change 8, 364–365. https://doi.org/10.1038/s41558-018-0154-5.

Tripathy, K.P., Mishra, A.K., 2023. How unusual is the 2022 European compound drought and heatwave event? Geophys. Res. Lett. 50, e2023GL105453 https://doi.org/10.1029/2023GL105453.

Ukkola, A.M., Kauwe, M.G.D., Pitman, A.J., Best, M.J., Abramowitz, G., Haverd, V., Decker, M., Haughton, N., 2016. Land surface models systematically overestimate the intensity, duration and magnitude of seasonal-scale evaporative droughts. Environ. Res. Lett. 11, 104012 https://doi.org/10.1088/1748-9326/11/10/104012.

van der Wiel, K., Selten, F.M., Bintanja, R., Blackport, R., Screen, J.A., 2020. Ensemble climate-impact modelling: extreme impacts from moderate meteorological conditions. Environ. Res. Lett. 15, 034050 https://doi.org/10.1088/1748-9326/ab7668.

Vautard, R., Kadygrov, N., Iles, C., Boberg, F., Buonomo, E., Bülow, K., Coppola, E., Corre, L., van Meijgaard, E., Nogherotto, R., Sandstad, M., Schwingshackl, C., Somot, S., Aalbers, E., Christensen, O.B., Ciarlo, J.M., Demory, M.-E., Giorgi, F.,

Jacob, D., Jones, R.G., Keuler, K., Kjellström, E., Lenderink, G., Levavasseur, G., Nikulin, G., Sillmann, J., Solidoro, C., Sørland, S.L., Steger, C., Teichmann, C., Warrach-Sagi, K., Wulfmeyer, V., 2021. Evaluation of the large EURO-CORDEX regional climate model ensemble. J. Geophys. Res. Atmospheres 126, e2019JD032344. https://doi.org/10.1029/2019JD032344.

Wable, P.S., Jha, M.K., 2018. Application of Archimedean copulas to the impact assessment of hydro-climatic variables in semi-arid aquifers of western India. Hydrogeol. J. 26, 89–108. https://doi.org/10.1007/s10040-017-1636-7.

Yin, D., Roderick, M.L., Leech, G., Sun, F., Huang, Y., 2014. The contribution of reduction in evaporative cooling to higher surface air temperatures during drought. Geophys. Res. Lett. 41, 7891–7897. https://doi.org/10.1002/2014GL062039.

Yuan, W., Cai, W., Chen, Y., Liu, Shuguang, Dong, W., Zhang, H., Yu, G., Chen, Z., He, H., Guo, W., Liu, D., Liu, Shaoming, Xiang, W., Xie, Z., Zhao, Z., Zhou, G., 2016. Severe summer heatwave and drought strongly reduced carbon uptake in Southern China. Sci. Rep. 6, 18813 https://doi.org/10.1038/srep18813.

Yuan, W., Zheng, Y., Piao, S., Ciais, P., Lombardozzi, D., Wang, Y., Ryu, Y., Chen, G., Dong, W., Hu, Z., Jain, A.K., Jiang, C., Kato, E., Li, S., Lienert, S., Liu, S., Nabel, J.E. M.S., Qin, Z., Quine, T., Sitch, S., Smith, W.K., Wang, F., Wu, C., Xiao, Z., Yang, S., 2019. Increased atmospheric vapor pressure deficit reduces global vegetation growth. Sci. Adv. 5 https://doi.org/10.1126/sciadv.aax1396.

Zhang, W., Koch, J., Wei, F., Zeng, Z., Fang, Z., Fensholt, R., 2023. Soil moisture and atmospheric aridity impact spatio-temporal changes in evapotranspiration at a global scale. J. Geophys. Res. Atmospheres 128, e2022JD038046. https://doi.org/10.1029/2022JD038046.

Zhou, H., Shao, J., Liu, H., Du, Z., Zhou, L., Liu, R., Bernhofer, C., Grünwald, T., Dušek, J., Montagnani, L., Tagesson, T., Black, T.A., Jassal, R., Woodgate, W., Biraud, S., Varlagin, A., Mammarella, I., Gharun, M., Shekhar, A., Buchmann, N., Manco, A., Magliulo, E., Billesbach, D., Silberstein, R.P., Ohta, T., Yu, G., Chen, Z., Zhang, Y., Zhou, X., 2021. Relative importance of climatic variables, soil properties and plant traits to spatial variability in net CO2 exchange across global forests and grasslands. Agric. For. Meteorol. 307 https://doi.org/10.1016/J.AGRFORMET.2021.108506.

Zhou, S., Park Williams, A., Berg, A.M., Cook, B.I., Zhang, Y., Hagemann, S., Lorenz, R., Seneviratne, S.I., Gentine, P., 2019a. Land–atmosphere feedbacks exacerbate concurrent soil drought and atmospheric aridity. Proc. Natl. Acad. Sci. U. S. A 116, 18848–18853. https://doi.org/10.1073/PNAS.1904955116.

Zhou, S., Zhang, Y., Park Williams, A., Gentine, P., 2019b. Projected increases in intensity, frequency, and terrestrial carbon costs of compound drought and aridity events. Sci. Adv. 5, eaau5740 https://doi.org/10.1126/sciadv.aau5740.

Zscheischler, J., Seneviratne, S.I., 2017. Dependence of drivers affects risks associated with compound events. Sci. Adv. 3 https://doi.org/10.1126/sciadv.1700263.

Zweifel, R., Sterck, F., Braun, S., Buchmann, N., Eugster, W., Gessler, A., Häni, M., Peters, R.L., Walthert, L., Wilhelm, M., Ziemińska, K., Etzold, S., 2021. Why trees grow at night. New Phytol. 231, 2174–2185. https://doi.org/10.1111/NPH.17552.